MET.O.14

METEOROLOGICAL OFFICE
BOUNDARY LAYER RESEARCH BRANCH
TURBULENCE & DIFFUSION NOTE

T.D.N. No.154

A Finite-Differencing scheme for use in a 1-D Mixing length model of the Atmospheric Boundary Layer.

by

N.S.Callen.

April 1984.

Introduction

Often the initial conditions used for 2-D integrations in boundary layer modelling are the steady state one-dimensional solutions of the momentum and buoyancy equations. Unfortunately, the iterative procedure used to obtain these solutions, discussed in Mason and Sykes (1980), does not remain numerically stable with increased grid resolution. Such increased resolution is needed to represent the region of an inversion in a convective boundary layer. To overcome this, the use of a time marching scheme is considered.

1. The Model

The one-dimensional momentum and buoyancy equations may be written as

$$\frac{\partial u}{\partial t} = f(v - v_g) + \frac{\partial}{\partial z}\tau_{13} \qquad (1.1a)$$

$$\frac{\partial v}{\partial t} = -f(u - u_g) + \frac{\partial}{\partial z}\tau_{23} \qquad (1.1b)$$

$$\frac{\partial B}{\partial t} = \gamma(B - B_0(z)) + \frac{\partial}{\partial z}H_3 \quad ; \; 0 \leq z \leq D \qquad (1.1c)$$

where f is the coriolis parameter, τ_{ij} is a turbulent Reynolds stress tensor, H_i is a turbulent buoyancy flux vector, $B \; (= g(T-\bar{T})/\bar{T})$ represents the fluid buoyancy, $\gamma(B - B_0(z))$ represents a damping to some prescribed state $B_0(z)$ on a time scale γ^{-1} and D is the depth of the model domain. The form of the buoyancy equation is discussed in more detail in Mason & Sykes (1982). In this work only its representation in a finite differencing scheme is important.

a) Turbulence Parametrization

To parametrize τ_{ij} and H_i a simple mixing length model closure hypothesis is considered following Smagorinsky (1963).

$$\tau_{ij} = \nu\left(\frac{\partial u_i}{\partial x_j} + \frac{\partial u_j}{\partial x_i}\right) \qquad (1.2a)$$

$$H_i = \nu \frac{\partial B}{\partial x_i} \qquad (1.2b)$$

where $\nu = l(z) \times (l(z)S)$, $l(z)$ is a prescribed mixing length scale and

$$S = \left\{ \tfrac{1}{2}\left(\frac{\partial u_i}{\partial x_j} + \frac{\partial u_j}{\partial x_i}\right)\left(\frac{\partial u_i}{\partial x_j} + \frac{\partial u_j}{\partial x_i}\right) \right\}^{1/2} \qquad (1.3)$$

From the turbulent kinetic energy balance equation, the buoyancy effects imply a velocity scale of $l(z) S (1-Ri)^{1/2}$. Accordingly, in the unstable region of the flow, the factor $(1-Ri)^{1/2}$ was included in the definition of γ.

So that $l(z)$ may be smoothly changing through the various regions of the flow it is formulated as

$$\frac{1}{l(z)} = \frac{(1-Ri)^{1/4}\,\phi}{K(z+z_0)} + \frac{1}{l_0(z)\,\psi} \qquad ; Ri < Ri_{CRIT} \qquad (1.4a)$$

$$l(z) \sim 0 \qquad ; Ri \geq Ri_{CRIT} \qquad (1.4b)$$

where z_0 is the roughness length, k is the von Karman constant, $l_0(z)$ the background mixing length and Ri, the Richardson number, is defined as $\frac{\partial B}{\partial z} / S^2$. The choice of the empirical functions ϕ and ψ is discussed in Mason and Sykes (1982) and they take the values

$$\phi = \begin{cases} (1-4\alpha Ri)^{1/4} & Ri < 0 \\ 1 & 0 \leq Ri < Ri_{CRIT} \end{cases} \qquad (1.5)$$

$$\psi = \begin{cases} 1 & Ri < 0 \\ (1-\beta Ri) & 0 \leq Ri < Ri_{CRIT} \end{cases} \qquad (1.6)$$

where $\alpha = 3, \beta = 3, Ri_{CRIT} = \frac{1}{\beta} = \frac{1}{3}$.

b) Boundary Conditions

The upper boundary is positioned high enough to effectively simulate an infinite depth. This boundary is a stress-free rigid lid, i.e.

$$\frac{\partial u}{\partial z} = \frac{\partial v}{\partial z} = 0 \; ; \; \frac{\partial B}{\partial z} = \frac{\partial B_0}{\partial z} \qquad \text{on } z = D \qquad (1.7)$$

where $\frac{\partial B_0}{\partial z}$ is the initial buoyancy gradient.

On the lower boundary, conditions consistent with $l(z)$ are derived assuming that the flow between the surface and the first grid point is in local equilibrium. It is assumed that

$$\frac{\partial V}{\partial z} = \frac{u_*}{k(z+z_0)} \phi \qquad (1.8)$$

$$\frac{\partial B}{\partial z} = \frac{H_*}{k(z+z_0)} \phi \qquad (1.9)$$

where z_0 is the specified roughness length, u_* the square root of the surface stress; V the total velocity at the lowest gridpoint and $H_* = b/u_*$ where b is the specified buoyancy flux and ϕ is defined as in equation (1.5). The value of u_* is calculated using an iterative procedure involving the integration of the above equations.

c) Numerical grid

Variables are stored on a staggered grid which is stretched in the vertical (see fig 1). The variables u, v and B are stored on the zN grid whereas their respective vertical gradients $\left(\text{i.e. } \frac{\partial u}{\partial z}, \frac{\partial v}{\partial z}, \frac{\partial B}{\partial z}\right)$ and therefore ν and Ri are stored on the z grid.

2. Finite difference scheme

Since a steady state solution of the momentum and buoyancy equations is eventually required, any explicit finite-differencing scheme seemed unlikely to prove beneficial. Although explicit methods are easy to program and require few computations at each timestep they are restricted to very small timestep intervals, Both the classical FTCS (Forward-time Centred-space) and the Dufort-Frankel methods become numerically unstable with increasing Δt.

In view of this, an implicit scheme was adopted but incorporated into it is the facility to use explicit terms if necessary. It is based on the "method of weighted averages" used by Crandall (1955). The finite difference approximation to equations (1.1a) - (1.1c) at the gridpoint (k,t) is

$$\frac{S_K^{t+1} - S_K^{t-1}}{2\Delta t} = F_K^t + \beta \left\{ \frac{\nu_K^t \left(S_{K+1}^{t+1} - S_K^{t+1}\right)}{\Delta zN_{K+1}} - \frac{\nu_{K-1}^t \left(S_K^{t+1} - S_{K-1}^{t+1}\right)}{\Delta zN_K} \Big/ \Delta z_K \right\}$$

$$+ (1-\beta) \left\{ \frac{\nu_K^t \left(S_{K+1}^{t-1} - S_K^{t-1}\right)}{\Delta zN_{K+1}} - \frac{\nu_{K-1}^t \left(S_K^{t-1} - S_{K-1}^{t-1}\right)}{\Delta zN_K} \Big/ \Delta z_K \right\} \qquad (2.1)$$

where $2 \leq K \leq (KK-1)$; $t \geq 2$; $0 \leq \beta \leq 1$;

S denotes the variable, either u, v or β ; Δz and ΔzN are the grid intervals (see Fig. 1); ν is the viscosity and F represents the coriolis term in (1.1a) and (1.1b) and the damping term in (1.1c). The conditions mentioned in section 1.b are applied at the upper and lower boundaries.

Note that with a constant ν specified, in both space and time, and also constant grid intervals (ie $\Delta zN_{k+1} = \Delta zN_k = \Delta z_k = \Delta z_{k+1}$; $\forall k$) equation (2.1) reduces to a much more familiar form:

$$\frac{S_k^{t+1} - S_k^{t-1}}{2\Delta t} = F_k^t + \beta\left\{\frac{\nu\left(S_{k+1}^{t+1} - 2S_k^{t+1} + S_{k-1}^{t+1}\right)}{(\Delta z)^2}\right\} + (1-\beta)\left\{\frac{\nu\left(S_{k+1}^{t-1} - 2S_k^{t-1} + S_{k-1}^{t-1}\right)}{(\Delta z)^2}\right\} \qquad (2.2)$$

The scheme is effectively second-order accurate in both space and time; the central difference approximation having been used for both the first-order time derivative and the second-order spatial derivative. However, if necessary, either a weighted or simply averaged ($\beta = 1/2$) value of the diffusion term approximation, over a $2\Delta t$ time interval, can be used.

If the weighting factor $\beta = 1$ this method reduces to a fully implicit method except for the coriolis term, F, and the viscosity, ν. To include F or ν in an implicit form would make the scheme extremely difficult, if not impossible, to use.

If $\beta = 1/2$ the method becomes very similar to that due to Crank and Nicolson (1947). In their method to solve the one-dimensional diffusion equation, with no coriolis term and a constant viscosity, they define the finite difference approximations at the point ($k, t + 1/2\,\Delta t$).

If $\beta = 0$ a fully explicit method is defined but this case was not considered. To choose a value for β (for simplicity this was limited to either $1/2$ or 1) some trial integrations were performed and will be discussed later.

a. Method of solution

Equation (2.1) may be rewritten as

$$-a_K S_{K-1}^{t+1} + (1 + a_K + b_K) S_K^{t+1} - b_K S_{K+1}^{t+1}$$

$$= 2\Delta t F_K^t + \alpha a_K S_{K-1}^{t-1} + (1 - \alpha(a_K + b_K)) S_K^{t-1} + \alpha b_K S_{K+1}^{t-1} \qquad (2.3)$$

where $a_K = \dfrac{2\Delta t \beta \nu_{K-1}^t}{\Delta ZN_K \Delta Z_K}$, $b_K = \dfrac{2\Delta t \beta \nu_K^t}{\Delta ZN_{K+1} \Delta Z_K}$

and $\alpha = \dfrac{(1-\beta)}{\beta} \qquad (\beta \neq 0)$

Commencing with the fields at $t = 0$ and $t = 1$ ($S_K^1 = S_K^0$; $\forall K$), and then taking $t = 2, 3, \ldots$ in turn, the right hand side of equation (2.3) is known for $K = 2, \ldots, (KK-1)$. Application of the boundary conditions which define the values of S_1^{t+1} and S_{KK}^{t+1} then yields a set of simultaneous equations in the unknowns S_K^{t+1} ; $K = 2, \ldots, KK-1$.

These equations are solved using Gaussian elimination followed by back substitution. The resulting fields, S_K^{t+1} are used to find the new viscosity field, ν_K^{t+1} , for use at the next timestep.

To reduce the cumulative effects of rounding error all calculations in the Gaussian elimination and the back substitution are performed in double precision.

b. Some initial integrations

A comparison was made of the steady state solutions reached by the finite differencing scheme (with $\beta = 1/2$ and $\beta = 1$) and by the matrix inversion technique used by Mason & Sykes (1980).

The model was integrated from initial conditions, given below, using timesteps of i) 10 secs and ii) 2500 secs to reach a steady state in both neutral and unstable cases.

i) Neutral case

The velocity fields were initialised with a geostrophic wind of 10ms-1 (ie $U_g = 10$, $V_g = 0$) throughout the height of the model except at the surface. Since the differencing scheme requires known fields at the previous two timesteps the fields at a time $t = -\Delta t$ were set equal to those at time $t = 0$. This should have no effect on the eventual solution but a slight decoupling of the even and odd timestep was apparent in early runs so a timesmoothing factor of 0.5 was introduced at each timestep. All other fields were initialised at zero except for the viscosity at $z = 0$ which was determined from u_* (the square root of the surface stress), itself initialised at 0.4 ms-1.

A background mixing length, $l_0(z)$ of 40m was used, following Mason & Sykes (1982), and the value of other parameters used were z_0 = 0.1m, f = 10^{-4}s-1 and D = 10^4m. The grid resolution was ~15m near the surface increasing to 50m throughout the rest of the boundary layer and eventually reaching ~400m in the upper half of the model domain.

To reach the steady state solution given by the matrix inversion the integrations had to be performed for about 80 hours 'real-time' to attain an accuracy of ~10-2ms-1 throughout the velocity fields. At this time the

values of U* given by the matrix inversion and timemarching methods differed by ~10-3ms-1 and although inertial oscillations persisted they were ~10-4ms-1. The resulting fields are shown in figure 2.

No significant differences were apparent between the integrations where $\beta = 1$ and $\beta = 1/2$ nor where $\Delta t = 10$ secs and $\Delta t = 2500$ secs. It seemed that only the time evolution of u_* from the initial conditions might provide a suitable criterion as to the choice of β. This was left until integrations in unstable conditions were made.

ii) Unstable case

All fields and parameters were initialised as in the neutral case above except that a static stability, $\partial B_\sigma / \partial z$; of 10-4s-2 was used together with a specified buoyancy flux, b = 10-3m2s-3. The damping term coefficient, γ , in equation (1.1c) was chosen to ensure that the depth of the boundary layer, z_i , was about 10^3 m.

Results from the integrations again showed similar accuracy although a numerical problem was experienced just below the inversion. A high positive anomaly occurred in the viscosity field at this point but as in Mason & Sykes (1982) an under-relaxation of the change in viscosities prevented this problem. The resulting fields are shown in figure 3.

As mentioned above, the time evolution of u_* was considered. Figure 4 shows the evolution from the initial conditions for the first 10000 secs of each integration.

With such contrived initial conditions it is hardly surprising to find that the use of very large timesteps (eg 2500 secs, effectively halved to 1250 secs due to the 50% timesmoothing) gives highly erratic values of u* at the start of the integrations. The fully implicit method ($\beta = 1$) does seem to have coped rather better than the Crank-Nicolson ($\beta = 1/2$).

With $\Delta t = 10s$ the time evolutions for both methods are almost identical, being smooth but falling from a very high value for u_* of 0.82 ms-1 reached within 30 secs of the start. However, in under 1000 secs, all integrations have a value of u_* within a range ~10-2ms-1.

On the evidence of the above integrations there seems little to choose between the fully implicit and Crank-Nicolson methods. Noye (1978) noted that numerical solutions to the one-dimensional diffusion equation were invariably more accurate when $\beta = 1/2$. However, his system of equations was somewhat less complex with no coriolis term or variable viscosities.

Based solely on the time evolution of u_* the fully implicit method was chosen for future use although it was also noted that with $\beta=1$ the right hand side of equation (2.3) reduces to $2\Delta t F_k^t + S_k^{t-1}$ and much CPU time could therefore be saved.

c. Effects of variation in grid resolution about the inversion

Figure 5 shows the buoyancy profiles of two steady state solutions obtained using the matrix inversion technique. All the parameters used in the integrations are specified as in section b) above except for the geostrophic wind which is set at 10 and 20ms-1 in turn.

It is clear from the profiles that a sharp numerical discontinuity exists between two grid points (Δz = 50m) above the well mixed layer. Increasing the grid resolution in this region produced numerical instability using the matrix inversion technique so the timestepping routine was used in an attempt to resolve this feature.

Grid resolutions of 50m, 10m, 5m and 2m about the top of the boundary layer were used and figures 6-9 show the resulting fields where u_g = 20ms-1.

Increasing the resolution has smoothed the buoyancy profile and consequently the Richardson-Number profile quite noticeably, although no difference is apparent between the 5m and 2m integrations. Fortunately, increased resolution did not shift the discontinuity about (and therefore not resolve it!); a problem that was experienced using the matrix inversion technique.

It may be deduced that the discontinuity present with a 50m grid resolution is not a serious numerical problem and that it is just a coarse representation of the smoother, higher resolution profile.

d) Stability

No mention has so far been made of the method's stability requirements. The fully implicit method with no coriolis or damping term and a constant viscosity and grid resolution is unconditionally stable. However, the inclusion of an explicit term together with variable viscosities and variable grid resolutions imposes stability restrictions. These are not easily found by analytical means and Table 1 shows the maximum timestep, Δt_{IMP}, found empirically. Also shown in Table 1 are the corresponding max. timesteps, Δt_{EXP}, for the explicit FTCS method. These values were calculated explicitly from the viscosity field using the stability criterion

$$\Delta t_{EXP} \leq \text{MIN} \left[\frac{(\Delta z)^2}{4\nu} \right] \qquad (2.4)$$

where both Δz and ν vary with height.

The value of Δt_{IMP} for the 50m integration is possibly even higher than the 3000 secs stated, this being the largest Δt used. Relative to this large value the remaining values for Δt_{IMP} appear remarkably small. No investigation has been made into this as yet but the larger values of were obtained when a suitable stretching algorithm was used. The grid used for the 50m integration has an almost constant 50m value for Δz throughout the boundary layer. Increased smoothing of the grid used for the 10m integration was responsible for Δt_{IMP} rising from ~50 secs to ~100 secs. In all integrations a maximum of 140 grid points was used - certainly not enough to produce a smoothly changing grid for a 5m or 2m resolution away from a boundary. This is an important point. The stability criterion (2.4) is unaffected by the rate of change of the grid intervals (Δz).

Since the rate of change of Δz imposes stability restrictions on the timestep in an implicit scheme it would not seem unreasonable to assume that similar restrictions could also be imposed on the timesteps in an explicit scheme. If this is so, the 5m and 2m values of Δt_{EXP} might be much smaller than indicated - probably less than the corresponding values of Δt_{IMP}. No further investigation was made into this anomaly.

The Crank-Nicolson method was also used for the 10m and 5m integrations to see if any improvement in Δt_{IMP} could be achieved. However, the results, as previously, showed very little difference from those obtained in Table 1.

e) Conclusions

The fully implicit method appears to be a satisfactory means of reaching a steady state solution. It also allows for investigation into the time evolution of the vertical profiles. The stability restrictions of

the method certainly require further investigation if high resolutions are to be used. However, with the coarser resolutions very large timesteps are possible without any apparent loss of accuracy.

Grid Resolution About the Top of the boundary layer	Max Timestep (secs) Δt_{IMP}	Max Timestep (secs) Δt_{EXP}
50m	3000+	~25
10m	~100	~14
5m	~10	~9
2m	~2	~7

Table 1 Empirically derived maximum timesteps, Δt_{IMP}, for the fully implicit method and theoretically derived max. timesteps, Δt_{EXP}, for the FTCS method.

References

Crandall, S. H. 1955 "An optimum implicit recurrence formula for the heat conduction equation". Quarterly of App. Maths. 13 pp 318-320.

Crank, J. & Nicolson, P. 1947 "A practical method for numerical evaluation of solutions of partial differential equations of the heat conduction type". Proceeding of the Cambridge Philosophical Soc. 43, No 50, pp 50-67.

Mason, P. J. & Sykes, R. I. 1980 "A two dimensional numerical study of horizontal roll vortices in the neutral atmospheric boundary layer". Quart. J.R. Met. Soc. 106 pp 351-366.

Mason, P. J. & Sykes, R. I. 1982 "A two dimensional numerical study of horizontal roll vortices in an inversion capped planetary boundary layer". Quart. J. R. Met. Soc. 108, 801-824.

Noye, J. 1978 "An introduction to finite difference techniques". Numerical simulation of fluid motion. Ed. J. Noye. pp 1-112.

Smagorinsky, J. 1963 "General circulation experiments with the primitive equations: 1 The basic experiments" Mon. Weath. Rev. 91 pp 99-164.

Figure 1. The stretched vertical grid. The variables U, V and B are stored on alternate grid points (ZN grid). The respective vertical gradients are stored on the remaining grid points (Z grid). $\Delta Z(K)$ and $\Delta ZN(K)$ represent the intervals Z(K) - Z(K-1) and ZN(K) - ZN(K-1) respectively.

Figure 2. Steady state profiles of v and u in netural case.

Ug = 10 ms-1

Z_o = 0.1 m

Figure 3. Steady state profiles of V, U and B in convective (unstable) case.

Ug = 10 ms-1

Z_o = 0.1 m

b = -10-3m2s-3

Figure 4. Time evolution of u* (unstable case)

Ug = 10ms-1

b = -10-3m2s-3

Z_o = 0.1 m

Figure 5. Steady state buoyancy profiles for unstable cases where Z_o = 0.1m.

b = -10-3m2s-3, Ug = (10ms-1 ——

(20ms-1 - - -

Figure 6. Steady state velocity profiles for unstable case where

Z_o = 0.1m

b = -10-3m2s-3

Ug = 20ms-1

ΔZ = 50, 10, 5, 2m about inversion

Figure 7. Steady state viscosity profiles for unstable case. Legend as for figure 6.

Figure 8. Steady state buoyancy profiles for unstable case. Legend as for figure 6.

Figure 9. Steady state Richardson no. profiles for unstable case. Legend as for figure 6.

Figure 1

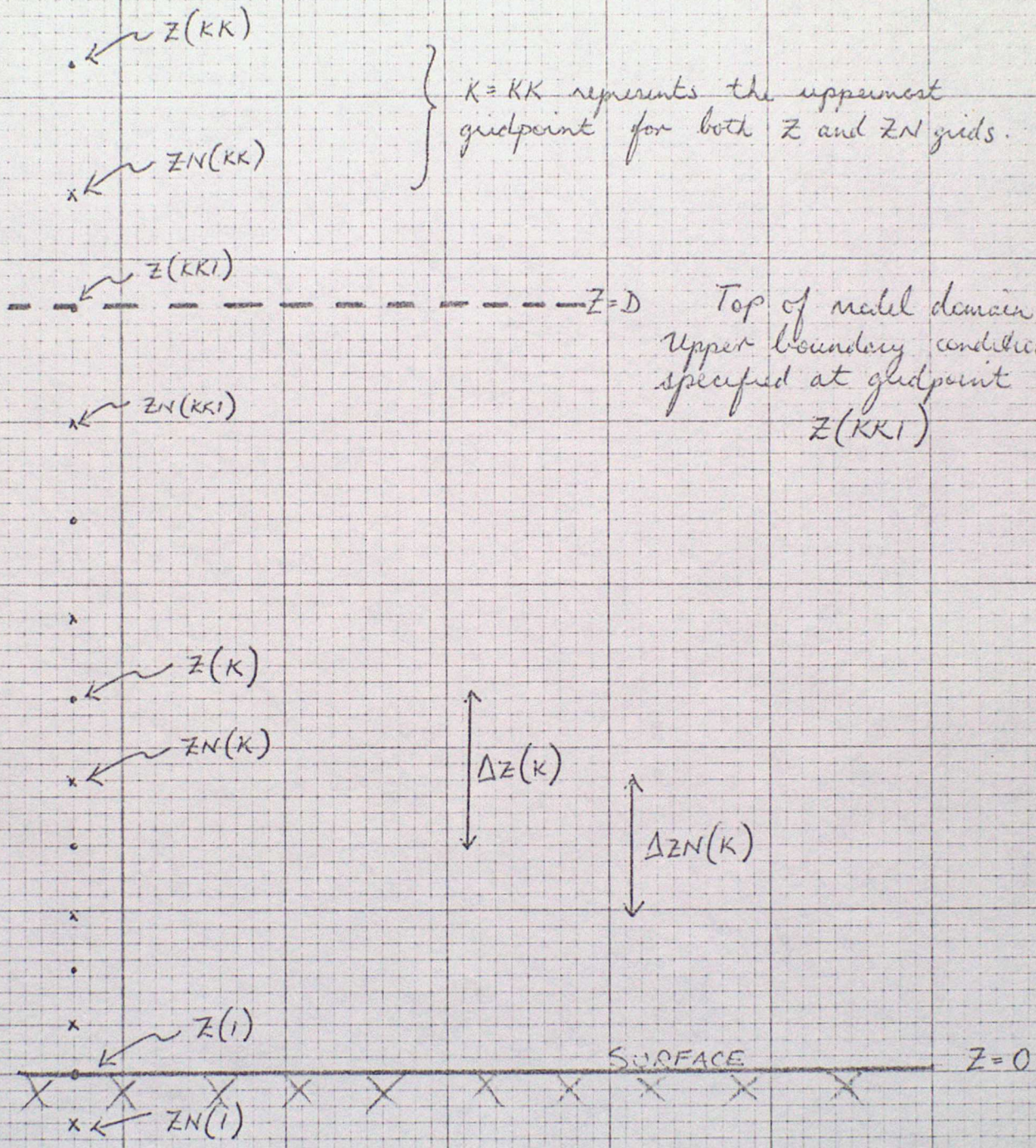

X represent ZN grid points - store U, V, B

• represent Z grid points - store ν, Ri, $\frac{\partial u}{\partial z}$, $\frac{\partial v}{\partial z}$, $\frac{\partial B}{\partial z}$

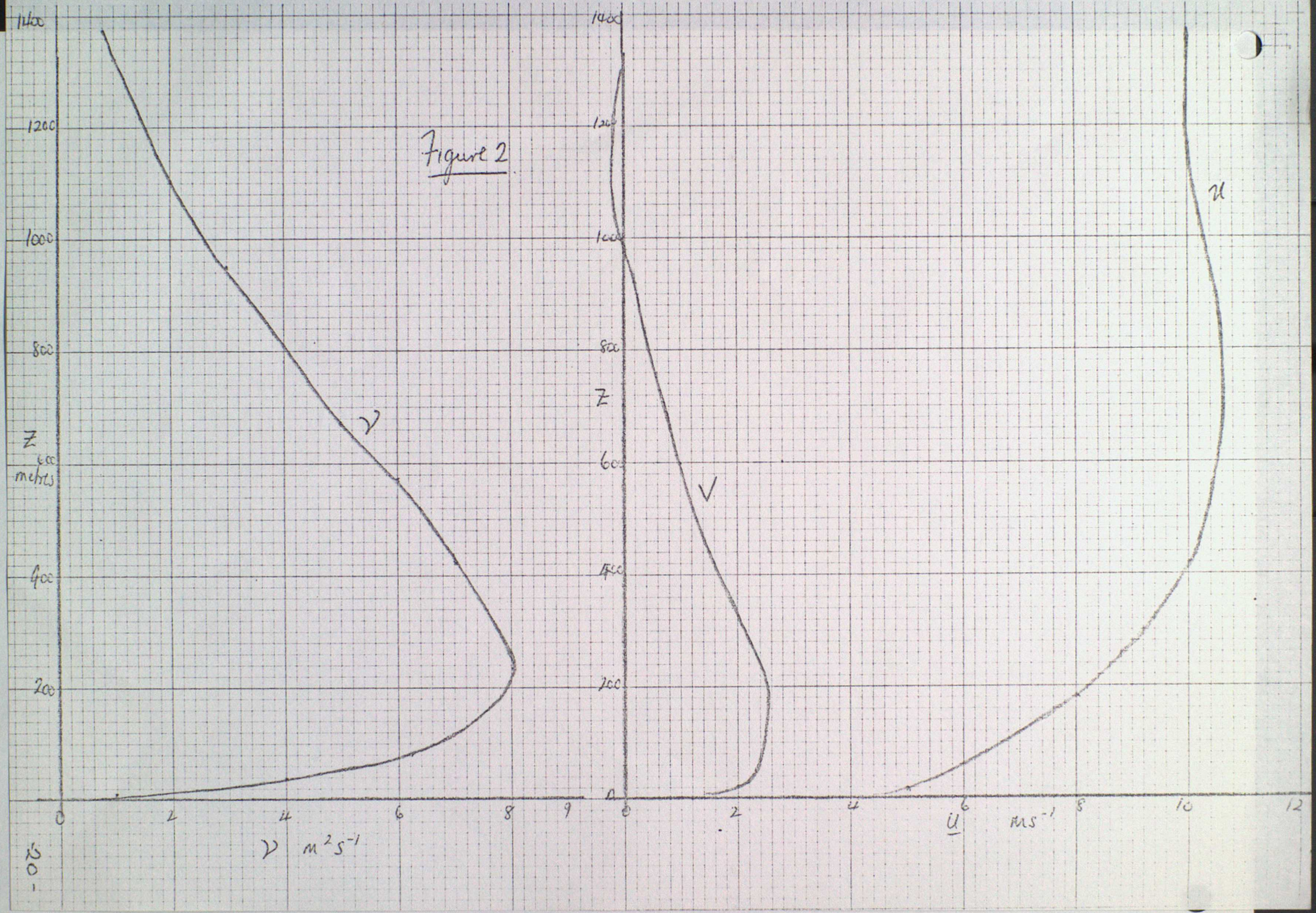
Figure 2
1400
1200
1000
800
600
400
200
0
Z
metres
V
2
4
6
8
10
12
$V \ m^2 s^{-1}$
$\underline{U} \ ms^{-1}$
U

Figure 3

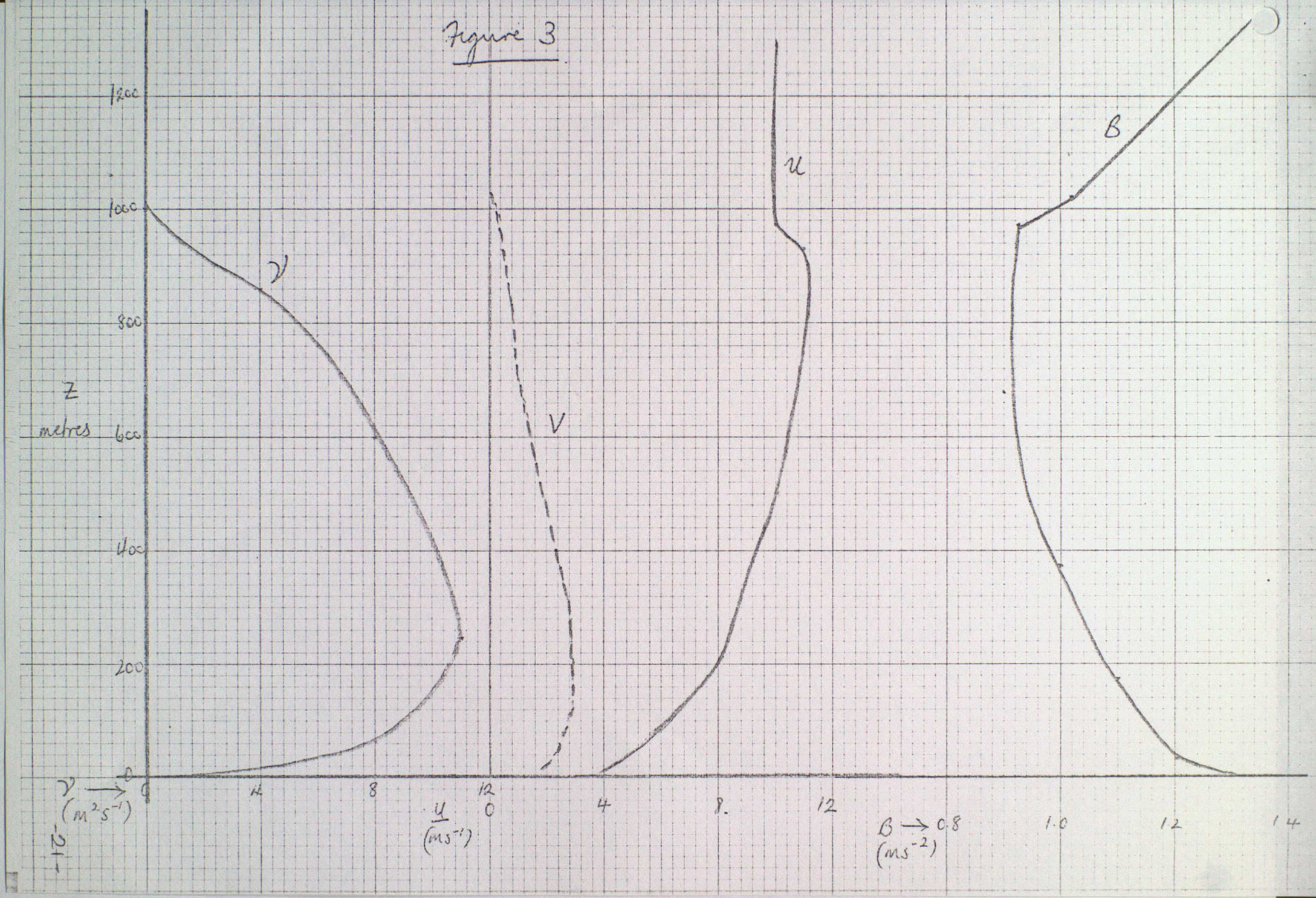
1200
1000
800
600
400
200
0
z
metres
v
V
u
B
0
4
8
12
0
4
8
12
0.8
1.0
1.2
1.4
v → (m² s⁻¹)
u (ms⁻¹)
B → (ms⁻²)

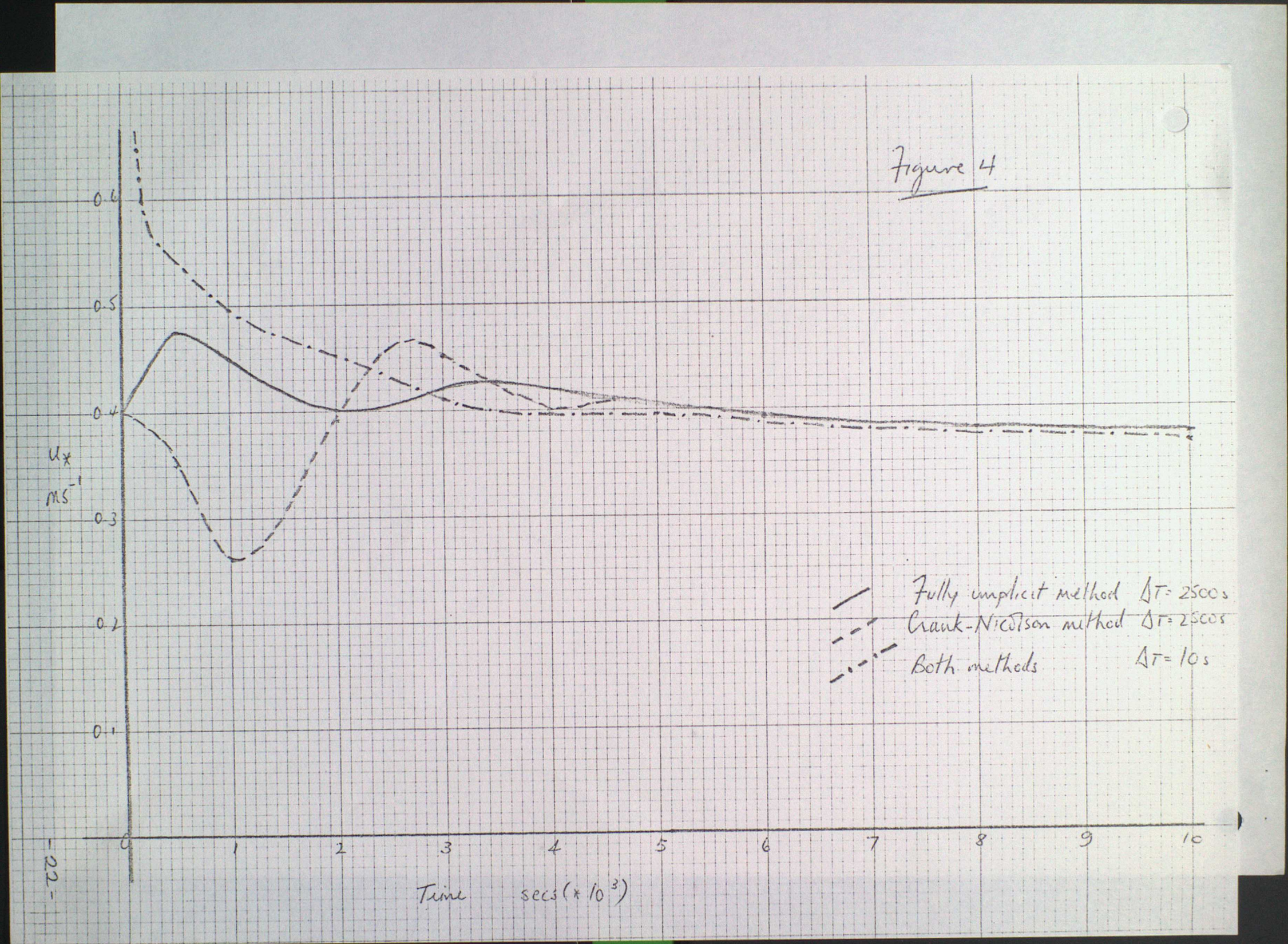
Figure 4
0.6
0.5
0.4
0.3
0.2
0.1
u_*
ms^{-1}
0
1
2
3
4
5
6
7
8
9
10
Time secs ($\times 10^3$)
Fully implicit method $\Delta T = 2500s$
Crank-Nicolson method $\Delta T = 2500s$
Both methods $\Delta T = 10s$

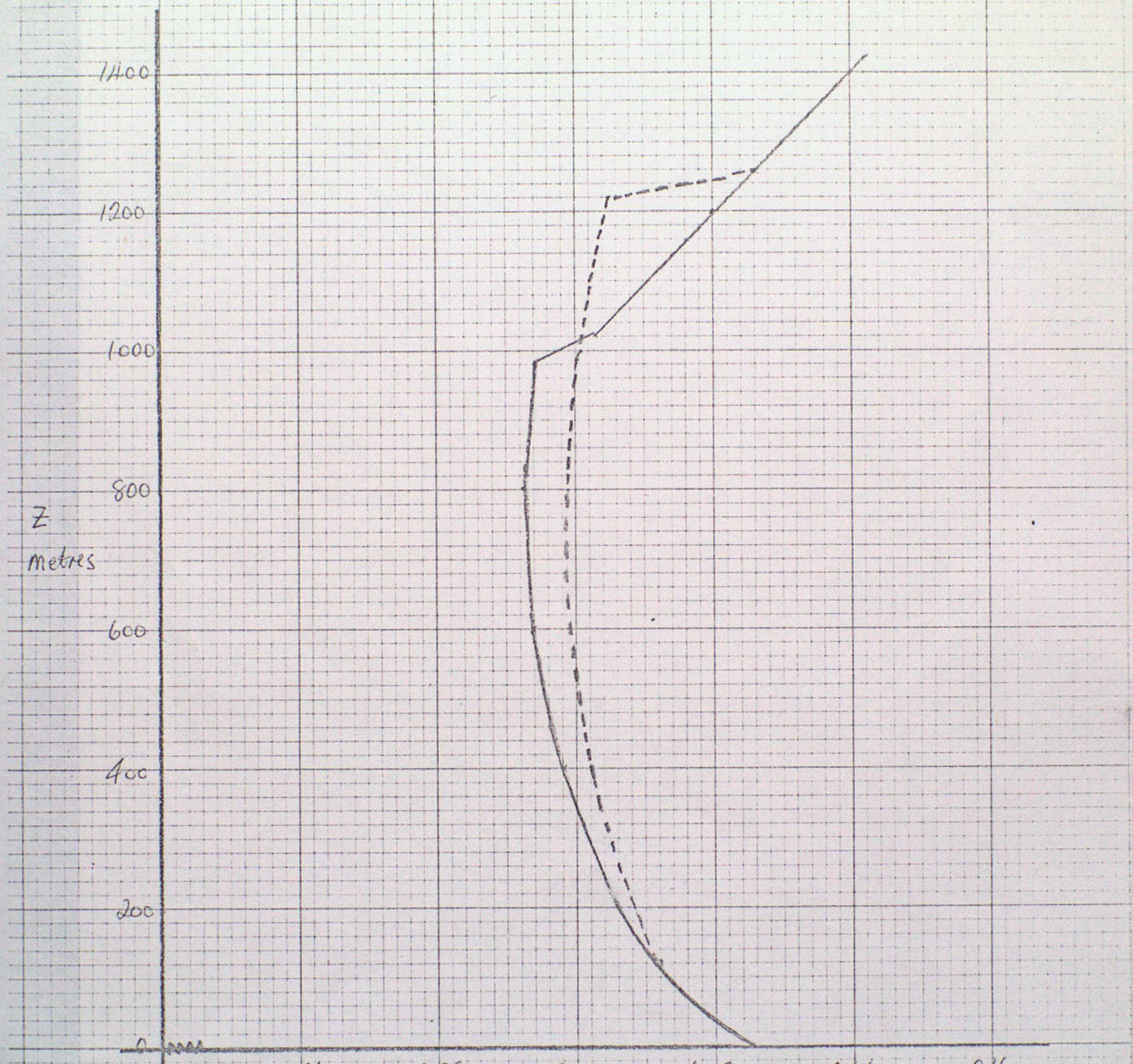
1400
1200
1000
800
Z
metres
600
400
200
0
0·06
0·08
0·10
0·12
0·14
0·16
B ms⁻²
10 ms⁻¹
20 ms⁻¹

Figure 5

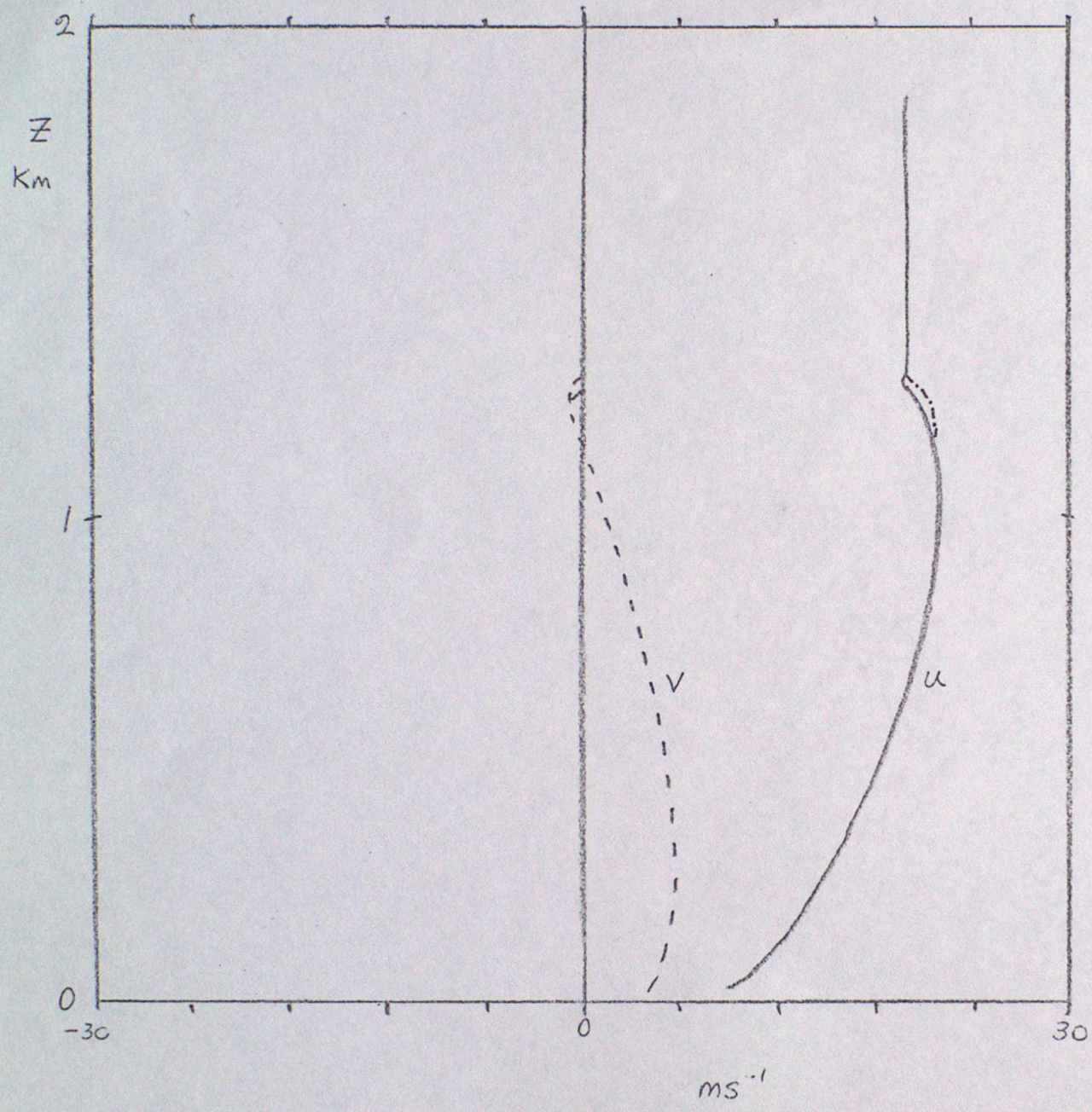

Figure 6

$\Delta z = 50m$ about inversion

u, v $\Delta z = 10m, 5m, 2m$ about inversion

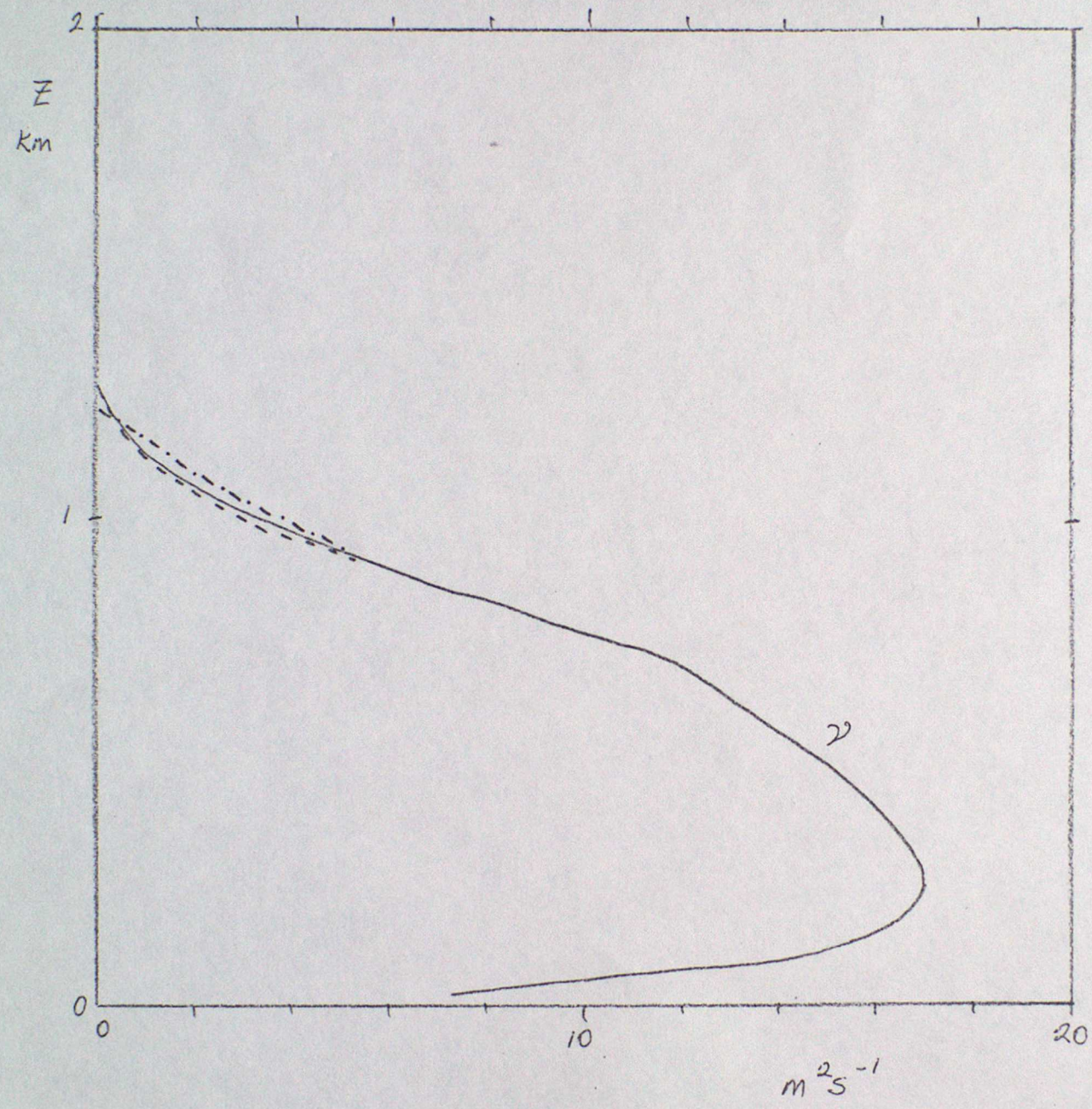

Figure 7

$\Delta z = 50m$ about inversion

$\Delta z = 10m$ about inversion

$\Delta z = 5m$ } about inversion
$= 2m$ }

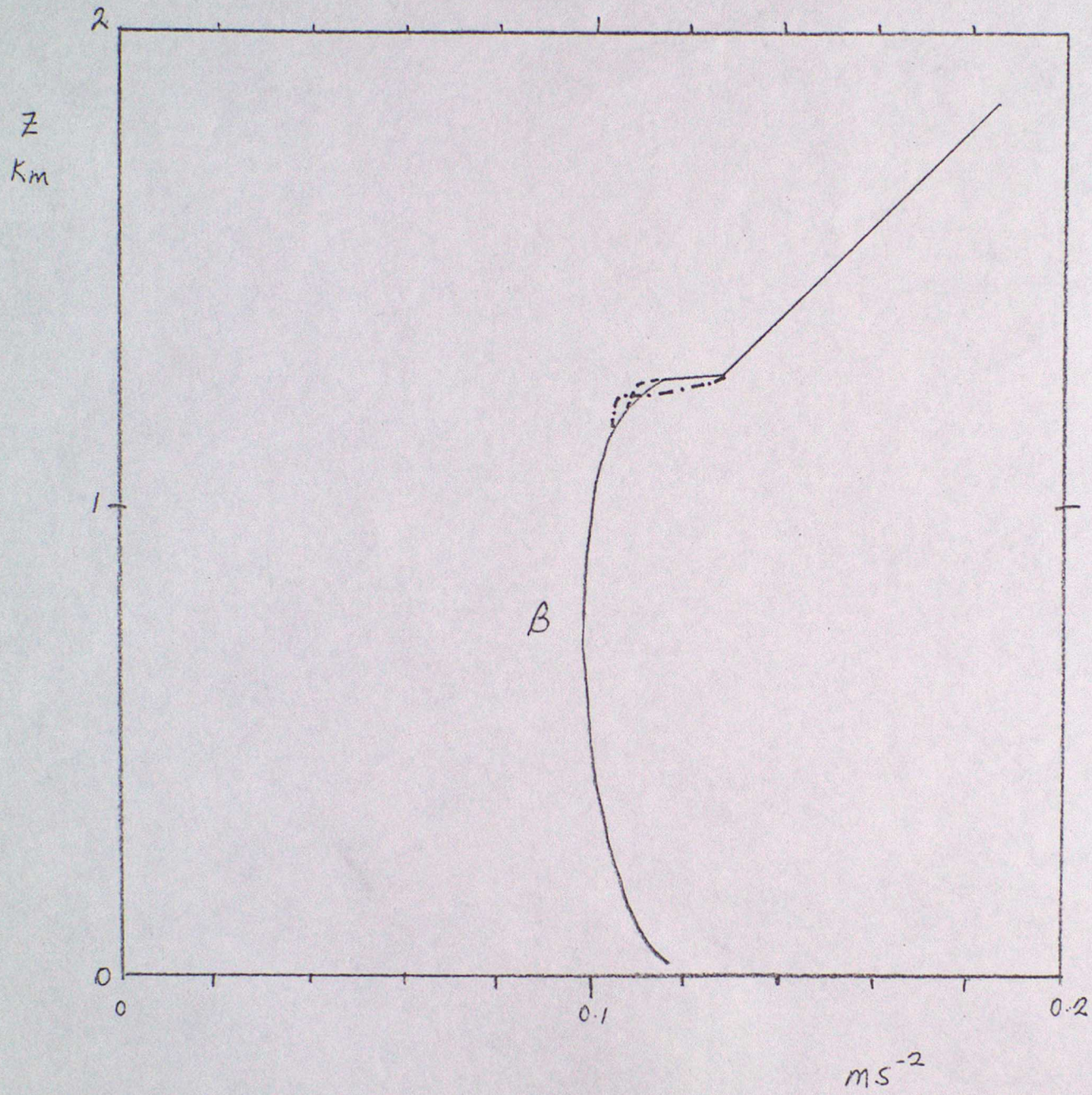

Figure 8

$\Delta z = 50m$ about inversion

$\Delta z = 10m$ about inversion

$\Delta z = 5m$, $\Delta z = 2m$ about inversion

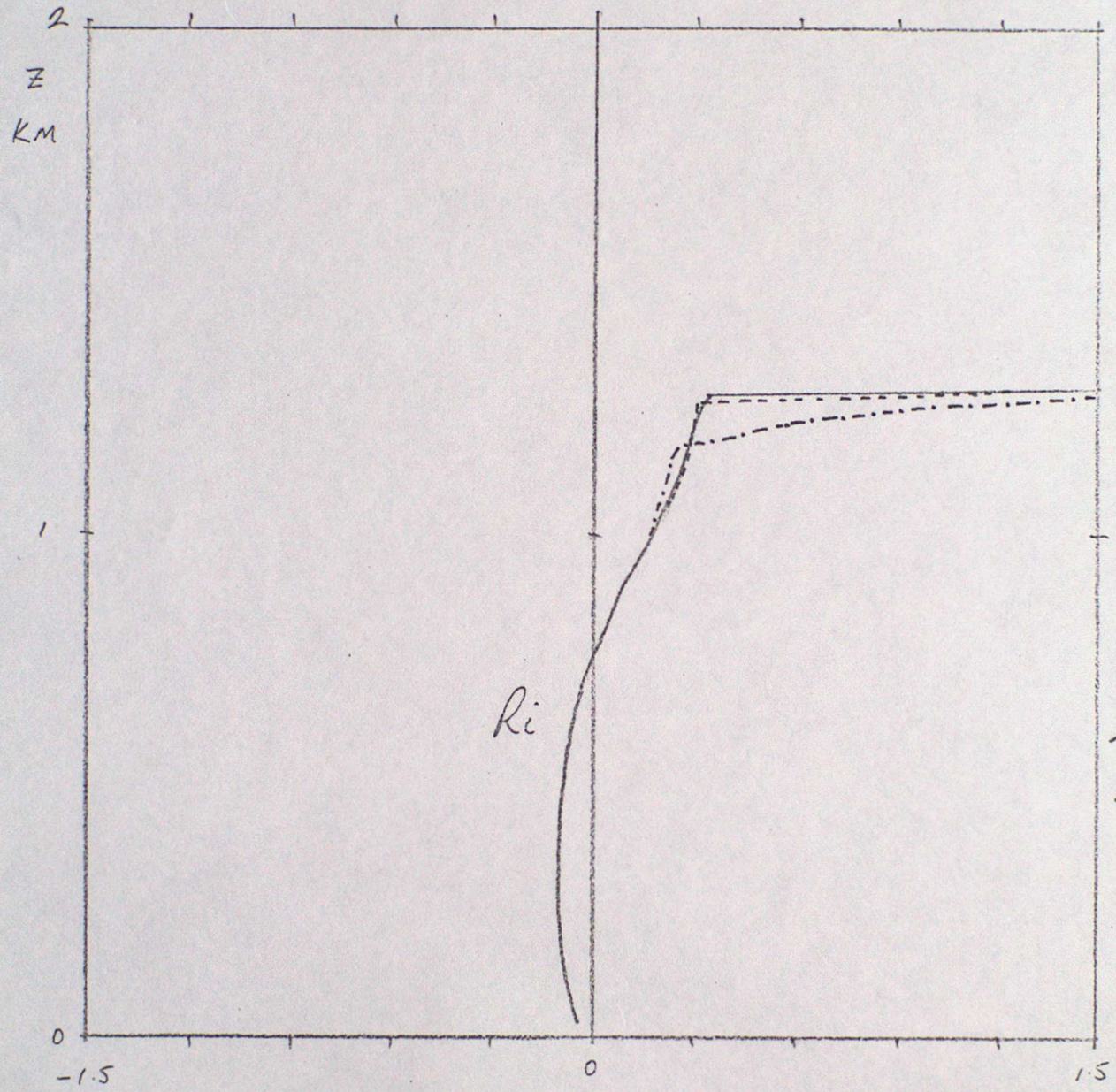

Figure 9

-·-·- Δz = 50m about inversion

- - - Δz = 10m about inversion

——— Δz = 5m, 2m about inversion